EXPLOSIVE SHAPES IN SMOOTHED-PARTICLE HYDRODYNAMICS (SPH) METHOD FOR STRUCTURAL ANALYSIS OF CONCRETE MEMBERS

Daniel Jindra*[,1], Petr Hradil[1], Jiří Kala[1]

*Jindra.d@fce.vutbr.cz
[1] Brno University of Technology, Faculty of Civil Engineering, Institute of Structural Mechanics, Veveří 331/95 602 00 Brno, Czech Republic

Abstract
The study compares performances of numerical finite element (FEM) analyses of simply supported concrete slabs reinforced by BFRP bars (basalt fibre reinforced polymer) exposed to close-range (1 m distance) explosions. A sensitivity study of slab deflection and reinforcement strain on various shapes of TNT charges is conducted. Smoothed-particle hydrodynamics (SPH) method is used to model the geometry of the TNT charges (variously rotated cylinders, cubes and spheres), detonation and interaction with the concrete slab, which is modelled by Lagrangian mesh. Karagozian and Case (K&C) nonlinear material model is used for concrete slabs exposed to high-velocity impact load. Finite element analyses have been conducted in explicit solvers suitable for high strain rates. The results of numerical simulations are compared with physical experiment data obtained from the scientific literature.

Keywords
Blast loading, concrete slab, explicit numerical analysis, smoothed-particle hydrodynamics (SPH)

1 INTRODUCTION

Many structures are required to retain their structural resistance while exposed to extreme load, e.g. aeroplane crash into the shell of a nuclear reactor, as modelled by Králik [1]. Water dams and bridge pylons might be exposed to crash of heavy traffic. Both the military defence structures, and all key infrastructure (bridges, dams, and plants) are often required to withstand the impacts of conventional weapon projectiles, or high-velocity pressure blast waves after explosions of conventional weapons, natural gas or other chemical products. Advanced tools of modern calculation technology [2] offer feasible numerical modelling and analysis of these high-velocity impact phenomena. Utilizing advanced numerical simulations, the design of structures might be optimized in order to improve the structural resistance, decreasing the number of physical experiments and the overall cost of the optimization process. Several approaches to modelling the blast load are available.

The blast wave effects might be considered as a time-dependent pressure load which is applied on the exposed surface of the structure modelled by a Lagrangian mesh of finite elements. The time dependency of pressure load is derived from empirical equations [3], [4] based on numerous experimental data. Input parameter values are available in the literature [5]. This simplified approach is referred to under “load blast enhanced”, abbreviation “LBE” in LS-Dyna [2] explicit solver, where it is implemented for commercial use.

In cases where the simplified approach does not offer the required features, such as the interference of several blast pressure waves from more epicentres, or analysis of more complex structural geometries, it is possible to use more advanced methods which enable model the propagation of the pressure waves in the surrounding environment (air, water) itself. An example of such a method is the “Arbitrary Lagrangian Eulerian” (ALE) method, where the exposed structure is modelled by Lagrangian mesh, and the surrounding domain by multi-material ALE mesh (MMALE) [2]. This method is more robust but has significantly larger requirements for CPU time. Additional inputs are required to be defined, such as the equation of state (EOS) [6] parameters for explosive material and surrounding air, and the material parameters for the explosive itself [7], [8].

If the blast epicentre is at a larger distance from the exposed structure, it is possible to combine these two approaches (LBE and ALE) to decrease computational demands. In this combined method, the ALE mesh of the air domain is modelled only in the closest structure surrounding it. The exterior surface of this air domain which faces the blast epicentre is modelled by special ambient elements [2]. These are loaded by the empirical pressure-time functions (LBE). Based on the load pressure data, these ambient elements determine the thermodynamic state data for the subsequent ALE air domain. The particle velocity and density are determined by Rankine-Hugoniot

DOI 10.13164/juniorstav.2024.24007

relations [9]. This combined method allows to analyse geometrically more complex surfaces exposed to pressure wave impact while decreasing computational time avoiding modelling the propagation of the pressure wave through the whole distance between the blast epicentre and the exposed surface of the structure. These methods are compared in several studies, e.g. by Tabatabaei et al. [10], or Slavik [11].

The explosive detonation might be modelled using the smoothed particle hydrodynamics (SPH) method. SPH was presented independently by Monaghan [12] and Lucy [13]. Even though the SPH method was originally introduced for astrophysical phenomena simulation, it has been already used in numerous different engineering tasks, e.g. in high-velocity impacts simulations by Libersky [14], exposure of rock and soil to blast pressure by Pramanik [15] and Chen [16]. Air blasts using the SPH method have been modelled by Schwer et al. [17] and Trajkovski [18] who also compared the performance with previously mentioned methods.

The material behaviour of concrete is different under various velocities of the load. Material parameters are often expressed in dependence on strain rates (change of strain in time). Higher concrete tensile and compressive strengths have been observed for larger strain rates [19]. Exposure of concrete structures to blast loading has been studied e.g. by Tai et al. [20], Zhao and Chen [21], [22], Thiagarajan et al. [23] and Dubec, et al. [24]. The behaviour of concrete under high-strain rates caused by high-velocity impact loads is still the object of continuous research.

This study presents numerical finite element (FEM) analyses of physical experiments recently published by Gao et al. [25], who studied the sea-water and sea-sand concrete slabs reinforced by basalt fibre-reinforced polymer (BFRP) exposed to close-range TNT blasts, and compared the performance with ordinary concrete BFRP slabs. In this paper, the analyses of ordinary concrete BFRP slabs are presented and discussed. Karagozian and Case (K&C) [26], a material model for a concrete slab is used, which is suitable when high strain rates are involved. The strain rate dependencies of concrete tensile and compressive strengths are defined in accordance with research by Malvar et al. [19]. Reinforcement strain rate effects are neglected, as in this case it appeared not to be applicable (explained further in the paper). If applicable, the reinforcement strain rate effects might be estimated based on the review by Malvar et al. [27] who summarizes the static and dynamic properties of steel bars.

The objective of this study is to compare the performances of various initial shapes of TNT explosives in numerical analysis using the SPH method and to conduct a basic sensitivity study. For all the analysed cases, the total mass of the explosive is the same, 0.4 kg in the 1 m stand-off distance above the exposed concrete slab mid-span. Various shapes of the TNT explosives are analysed: variously declined cylinders, cubes, and spheres. All the other assumptions (material parameters, time step size, mesh size) remain invariant. The results are compared with the experimental data [25], simplified approach analysis (LBE) and discussed. The paper provides additional know-how for the numerical analyses of structures exposed to high-velocity blast loads.

Experiments and a physical model

The physical experiments are described in detail by Gao et al. [25]. In the presented research study, the ordinary (plain) concrete slab noted by Gao et al. as BRPS1 [25] was numerically analysed. The average compressive strength of concrete class C40 was 49.34 MPa, based on tests of 6 cubes (150 mm) cured for 28 days at room temperature [25]. The tensile strength (at static strain rates) of the concrete was considered as 3 MPa, and Poisson's ratio was 0.2. Concrete slab dimensions were 50 mm in height (thickness), 500 mm in width and 1,100 mm in length. The slab was reinforced by BFRP bars Ø 6 mm in both directions in a regular grid with a span of 100 mm. Bars were located at the bottom surface with 10 mm of concrete cover, hence the effective depth of the slab was 37 mm. The physical tests of the BFRP reinforcement bars [25] have resulted in the average tensile strength of 1.53 GPa (Fig. 1 (a), based on [25], [28]) and the Young's elastic modulus of 57.68 GPa.

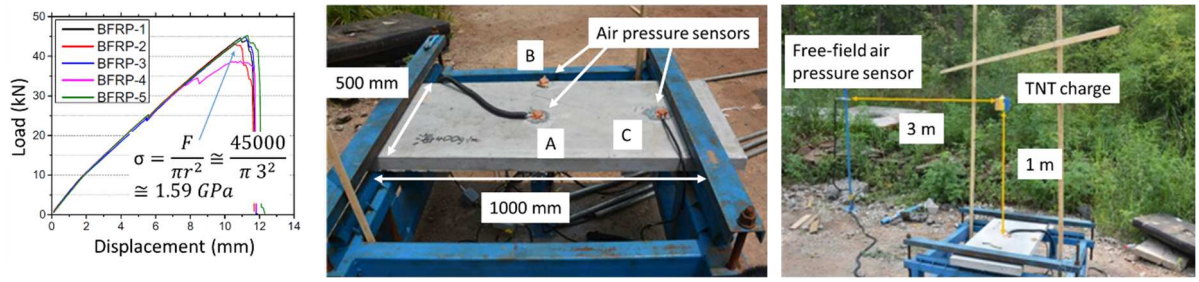

(a) (b) (c)

Fig. 1 (a) Tensile tests of the BFRP bars, Gao, Feng et al. [25],[28]; (b), (c) Experiment set-up.

DOI 10.13164/juniorstav.2024.24007

The experimental setup is depicted in Fig. 1 (b)). The concrete slab of a 1 m structural span was simply supported on a steel frame and secured by the frame from the top side to avoid the post-blast uplift at both edges. The TNT charge was located in the stand-off distance of 1 m above the mid-span of the slab. In this research, the variant with 0.4 kg of TNT was analysed (also 0.8 kg and 2.0 kg were tested by Gao et al. [25]). Before casting the concrete slab, a strain gauge was installed directly on the BFRP bar in the mid-span. Air pressure sensors were located on the top surface of the slab, and one free-field air pressure sensor was at 3 m distance from the charge (Fig. 1 (b), (c)).

2 NUMERICAL ANALYSES

Smoothed-Particle Hydrodynamics Method – SPH

This method is a mesh-free (Lagrangian) solver, originally developed for hydrodynamics. The governing equations of fluid dynamics in the form of partial differential equations were determined by interpolation from the particles. Discretized formulation derivation of the SPH method was divided into two steps.

The first step is called kernel approximation, equations (1) and (2). The arbitrary function and its gradient were introduced in dependence on smoothing length h and smoothing kernel function W (adopted as cubic B-spline [2]):

$$\langle f(x)\rangle = \int_{\Omega} f(x')W(x-x',h)dx' \tag{1}$$

$$\langle \nabla f(x)\rangle = -\int_{\Omega} f(x')\nabla W(x-x',h)dx' \tag{2}$$

In the second step, using equations (3) and (4), which was termed as particle approximation, the integral forms of the function and the function gradient were approximated by the summarization of the nearest particle values:

$$\langle f(x_i)\rangle = \sum_{j=1}^{N} f(x_j)W_{ij}\frac{m_j}{\rho_j} \tag{3}$$

$$\langle \nabla f(x_i)\rangle = -\sum_{j=1}^{N} f(x_j)\nabla W_{ij}\frac{m_j}{\rho_j} \tag{4}$$

where m_j and ρ_j are mass and density respectively. $W_{ij} = W(x_i - x_j,h)$.
For the explosive TNT material, the Jones Wilkins Lee (JWL) Equation of State (EOS) was used [6], where the pressure was defined as a function of the internal energy per volume E, and relative volume V, as in equation (5):

$$P = A\left(1-\frac{\omega}{R_1V}\right)e^{-R_1V} + B\left(1-\frac{\omega}{R_2V}\right)e^{-R_2V} + \frac{\omega E}{V} \tag{5}$$

where EOS parameters A, B, R_1, R_2, ω and also TNT material parameters such as Chapman-Jouguet Pressure (PCJ), detonation velocity, density and internal energy per reference volume $E0$ [2] were defined in accordance with [7], [8].

Simplified Blast Model – LBE method

The simplified approach is also known as "load blast enhanced" (LBE) in LS-Dyna [2]. The effects of the blast pressure wave were considered a time-dependent surface pressure load. This load was determined by the blast loading empirical function, equation (6), defined by Randers-Pehrson and Bannister [3]:

$$P(t) = P_r(t)\cos^2\theta + P_s(t)(1+\cos^2\theta - 2\cos\theta) \tag{6}$$

where θ is the angle of incidence, $P_s(t)$ and $P_r(t)$ [Pa] are time-dependent incident (free-air) and reflected overpressures respectively. Both pressures were defined in accordance with the Friedlander equation [4]. For the case of free-air overpressure $P_s(t)$ this equation was defined by equation (7) as:

$$P_s(t) = P_{so}\left(1-\frac{t}{t_o}\right)\cdot e^{-b\frac{t}{t_o}} \tag{7}$$

DOI 10.13164/juniorstav.2024.24007

where P_{so} is the peak incident (free-air) overpressure, in Pascals, b, is waveform decay coefficient [-], and t_o is the duration of the positive phase [s] (afterwards the overpressure wave, there is a wave of lower pressure). These parameters were determined based on scaled distance Z, equation (8), introduced by Hopkinson [29] and Cranz [30]:

$$Z = \frac{R}{W^{1/3}} \tag{8}$$

where W, in kilograms, is the equivalent mass of TNT, and R, in meters, is the distance from the blast epicentre. Values of these parameters in SI units might be obtained from the JRC technical report [5]. The analysed case of 0.4 kg of TNT in the 1 m stand-off distance resulted in a scaled distance of 1.357 m·kg$^{-1/3}$, and the contact time of the blast wave with the structure surface t_a was expected to be approximately 700 µs.

Experimental reference time-pressure data depicted in Fig. 2 (a)) were based on a study by Gao et al. [25]. Position of the sensor A is in the mid-span right beneath the TNT charge and sensor B is at the slab edge (Fig. 1 (b)). The experimental time-pressure curves were a rather nice match with the empirical estimations (equations (1), (2)), and the values of the pressure impulses i, in Pa·s, obtained by integration of these pressure-time curves approximately corresponded (280 ≈ 256 for sensor A; 270 ≈ 214 for sensor B, what is considered as a nice match).

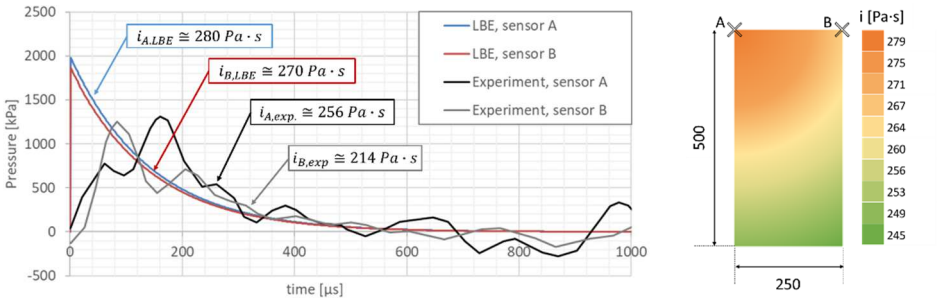

(a) (b)

Fig. 2 (a) Pressure-time experimental references and empirical estimations; (b) Estimation of the pressure impulse based on empirical approach – symmetric 1/4 of the slab.

Karagozian and Case (K&C) – Nonlinear Material Model for Concrete

K&C material model [26] is suitable for numerical analysis of concrete structures exposed to high strain rates. The first release of the material model is dated to the year 1994 [31]. In the second release, some additional aspects as shear dilation were implemented [32]. The third release [33] has introduced automatic parameter generation based on uniaxial compressive strength (used in this study). The dependence on finite element mesh geometry due to strain-softening of the K&C was reduced in 2010 [34]. More details are available in the K&C report [35] which describes the use and validation of this material model.

The K&C model is a constitutive model defined by three invariants using three shear failure surfaces: initial, maximal and residual. These surfaces are mutually independent, and the general definition is mathematically described by equation (9) as:

$$F_i(p) = a_{0i} + \frac{p}{a_{1i} + a_{2i}p} \tag{9}$$

where y, m and r are substituted for index i to describe the initial yield strength surface, maximum shear failure surface and residual failure surface respectively. Values of the parameters a_{ji} (j = 0,1,2; i = y, m, r) are required to be calibrated based on experimental data. Pressure p [Pa] is dependent on the first invariant of stress tensor I_1, described by the equation (10) as:

$$p = -\frac{I_1}{3} \tag{10}$$

The resultant failure surface was interpolated between the maximal and initial (defined by equation (11)) or between the maximal and residual (as in equation (12)) failure surface based on provided formulas:

DOI 10.13164/juniorstav.2024.24007

$$F(I_1,J_2,J_3) = r(J_3)\left[\eta(\lambda)\left(F_m(p) - F_y(p)\right) + F_y(p)\right] \leftrightarrow \lambda \leq \lambda_m \tag{11}$$

$$F(I_1,J_2,J_3) = r(J_3)\left[\eta(\lambda)\left(F_m(p) - F_r(p)\right) + F_r(p)\right] \leftrightarrow \lambda > \lambda_m \tag{12}$$

where I_1 is the first invariant of the stress tensor, J_2 and J_3 are the second and the third invariants of the deviatoric stress tensor. λ express modified effective plastic strain, $\eta(\lambda)$ is a function of internal damage dependent on λ, with values: $\eta(0) = 0$, $\eta(\lambda_m) = 1$, $\eta(\lambda > \lambda_m) = 0$. This means, that the failure surface begins at the initial yield strength surface, and reaches the maximum shear surface as λ is increasing to λ_m. Afterwards, the failure surface decreases to the residual surface for further increasing λ up to the value of λ_{max}. The relations between λ, λ_{max} and $\eta(\lambda)$ are calibrated based on experimental data. $r(J_3)$ is a scaling factor in the form of an equation by William Warnke [36], which expresses the dependence on J_3 in a way that the transition between brittle and ductile (under higher confinement) response is well described.

Strain Rates Material Dependency

The material strength parameters increased rapidly under high strain rates $\dot{\varepsilon}$. During the exposure to blast loads strain rates were in the range from 10 to 1000 s^{-1}, and the increase was about 100% for concrete compressive strength, and 600% for the concrete tensile strength [19]. The effect of strain rate on concrete parameters is expressed by dynamic increase factors *DIF*, noted *TDIF* for tensile strength increase and *CDIF* for the compressive strength increase, and the dependence on the strain rate $\dot{\varepsilon}$ [19] is expressed in the equations (13) to (16):

$$\frac{f_c}{f_{cs}} = CDIF = \left(\frac{\dot{\varepsilon}}{\dot{\varepsilon}_{cs}}\right)^{1{,}016\delta} \leftrightarrow \dot{\varepsilon} \leq 30s^{-1};\ CDIF = \beta\left(\frac{\dot{\varepsilon}}{\dot{\varepsilon}_{cs}}\right)^{\frac{1}{3}} \leftrightarrow \dot{\varepsilon} > 30s^{-1} \tag{13}$$

$$\delta = \frac{1}{5 + 0{,}75 \cdot f_{cu}};\ \log(\beta) = 6{,}156\,\delta - 2;\ f_{cu} = 1{,}205\,f_c \tag{14}$$

$$\frac{f_t}{f_{ts}} = TDIF = \left(\frac{\dot{\varepsilon}}{\dot{\varepsilon}_{ts}}\right)^{\alpha} \leftrightarrow \dot{\varepsilon} \leq 1s^{-1};\ TDIF = \gamma\left(\frac{\dot{\varepsilon}}{\dot{\varepsilon}_{ts}}\right)^{\frac{1}{3}} \leftrightarrow \dot{\varepsilon} > 1s^{-1} \tag{15}$$

$$\alpha = \frac{1}{1 + 8 \cdot \frac{f_c}{f_{co}}};\ \log(\gamma) = 6\,\alpha - 2;\ f_{co} = 10\ MPa \tag{16}$$

where f_c, in Pascal, is compressive strength at the dynamic strain rate $\dot{\varepsilon}$ in the range from $3 \cdot 10^{-5}$ to 300 s^{-1}, f_{cs}, in Pascal, is compressive strength at the static loading strain rate $\dot{\varepsilon}_{cs} = 3 \cdot 10^{-5}$ s^{-1}, and the relation is determined by parameters δ, β and concrete cubic strength f_{cu}. Analogically for tension, f_t, in Pascal, is tensile strength at the dynamic strain rate $\dot{\varepsilon}$ in the range from $1 \cdot 10^{-6}$ to 300 s^{-1}, f_{ts}, in Pascal, is tensile strength at static loading strain rate $\dot{\varepsilon}_{ts} = 1 \cdot 10^{-6}$ s^{-1}, and α γ parameters are involved.

For reinforcing material (BFRP bars), the increase in yield strength at higher strain rates was not considered, due to the fact that the maximal strain experimentally detected in a bar was 1.5% [25], which corresponds to stress of 865 MPa (E = 57.68 GPa), smaller than the tensile strength of 1.53 GPa with a brittle failure (Fig. 1 (a)), so there is no need to incorporate the dynamic increase factors for the BFRP bars. The material model in the numerical analyses was considered bilinear, with negligible hardening (linear elastic, ideal plastic), with a yield stress of 1.53 GPa. The strains are monitored carefully that are below 2.65%, which is the limit value at the tensile strength.

Finite Element Numerical Models

The geometry of the numerical finite element model is depicted in Fig. 3. The concrete slab was modelled by hexahedral 8 nodal solid elements with 3 translational degrees of freedom per each node (Fig. 3 (a)). The concrete solid elements were 10 mm cubes near the line supports at the edges. In the ¼ of structural span, the mesh of concrete solid elements was refined into rectangular prisms of 10 × 5× 5 mm (The element size of 10 mm along the width was kept). This mesh geometry was considered for all the analyses where the explosive was modelled by the SPH. One analysis for verification where the blast load was modelled by the simplified approach (LBE) used half the mesh size in all the 3 directions, hence cubes of 5 mm edge at the sides, and prisms of 5 × 2.5 × 2.5 mm in the mid-span. These mesh sizes were further noted as 10 × 5 and 5 × 2.5 respectively. In all the cases, the solid elements with constant stress formulation and hourglass control were used.

DOI 10.13164/juniorstav.2024.24007

Boundary conditions (deformation constraints) were applied to a layer of contact material elements (linear elastic steel). Linear elastic concrete material was defined for solid elements near these contact areas (Fig. 3 (a)). These boundary conditions were applied also from the upper surface of the concrete slab in order to simulate the supports of the steel frame (Fig. 1 (b)).

The reinforcing bars were modelled by Hughes-Liu formulation beam elements with cross-section integration [2]. This option is more robust, and suitable also for plastic materials, but demands more CPU time than formulation by Belytschko-Schwer, which is suitable only for linear materials [2] (and should be sufficient enough). However, the processing of the beam elements took always only below 0.7% of total CPU time, for the calculations including the SPH presented in this study, hence the simpler formulation would speed up the calculation only negligibly. The reinforcement mesh size was the same as the refined mesh in the mid-span of the slab (hence 5 mm for all the analyses using the SPH, and 2.5 mm for one case of the simplified LBE approach). Axial strain history was monitored in the middle of the longitudinal reinforcing bar on a beam element from the mid-span.

In addition to concrete slab discretization by Lagrangian mesh, the TNT explosive was also required to be discretized if modelled by the SPH particles (nodes). These nodes were required to be aligned in a regular cubic nodal grid, which was considered 1 mm for all the analysed cases (Fig. 3 (b)). Radial grids of SPH nodes were not suitable [2], as these would result in different distances of the neighbouring nodes. The exact dimensions of the 0.4 kg TNT block, as referred to by Gao et al. [25] was unknown to the authors of this study – even though it appears to be in either cubic or rectangular prism shape (Fig. 1 (c)).

The main objective of this study was to compare the influence of various shapes of the TNT explosive on the structural performance of the exposed concrete slab. For all the cases, the total mass of the TNT explosive was the same, 0.4 kg. The stand-off distance measured from the top surface of the exposed slab to the centre of gravity of the TNT explosive (no matter the shape) was 1 m for all the analysed cases. An example of a TNT explosive block in the shape of a cylinder (0.1 m height), which is vertically aligned (the axis of the cylinder is parallel to the normal of the upper surface of the slab) is depicted in Fig. 3 (b). Based on the TNT density, which was considered as 1,650 kg·m^{-3} [7], [8], the diameter of the cylinder was derived. The masses of all the SPH nodes of certain cases were the same and were derived from the total number of SPH nodes and the total weight of the TNT charge (0.4 kg). For some cases of TNT explosive shape, two variants of the blast epicentre were considered – either in the centre of gravity of the explosive volume (noted as #mid) or in the uppermost point of the explosive volume (noted as #up). If there were more uppermost points for a certain shape, the one in the middle was used. An example of the cylindrical shape of an explosive is depicted in Fig. 3 (b).

All the analysed cases of explosive shapes are summarized in the Tab. 1 of the next chapter. Several rotations of the explosive volumes in the space were also considered, for cylindrical, cubical and spherical shapes, as the nodal grid within the sphere might be rotated (Fig. 4). These rotations are defined by two angles, α_x and α_y, which are deviations of the vertical axis of the explosive volume (the one parallel with z axis of the global coordinate system) towards x and y directions of the global coordinate system respectively. An example is depicted for the case of cylindrical explosives in Fig. 3 (c). Note: the vertically aligned cylinder (such as in Fig. 3 (b)) was considered with rotations $\alpha_x = \alpha_y = 0°$.

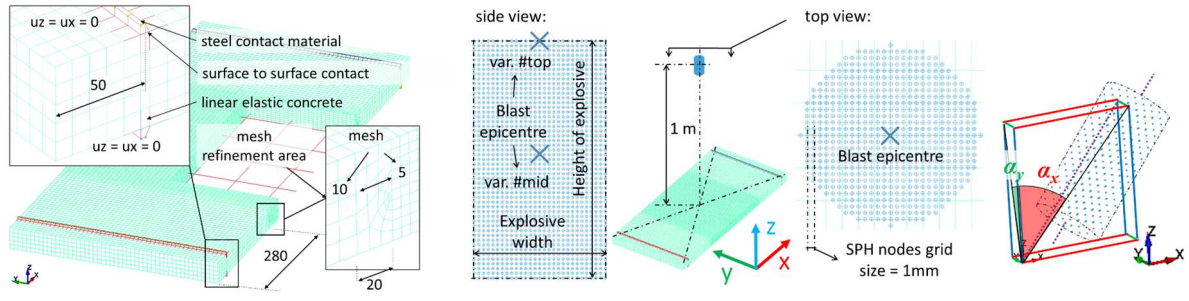

Fig. 3 Final element model: (a) detail of the concrete slab; (b) example of the cylindrical shape of the TNT explosive modelled by the SPH (vertically aligned); (c) possible rotations of the explosive shape.

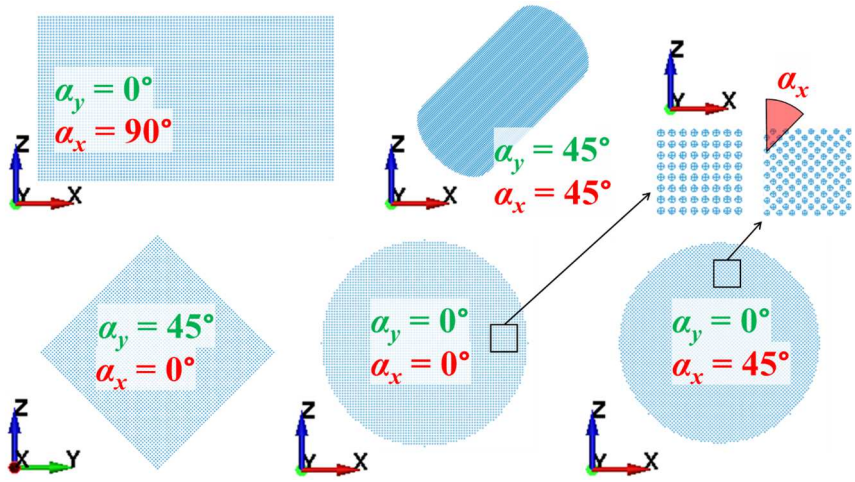

Fig. 4 Different shapes and rotations of TNT explosive volumes modelled by the SPH particles.

3 ANALYSES RESULTS

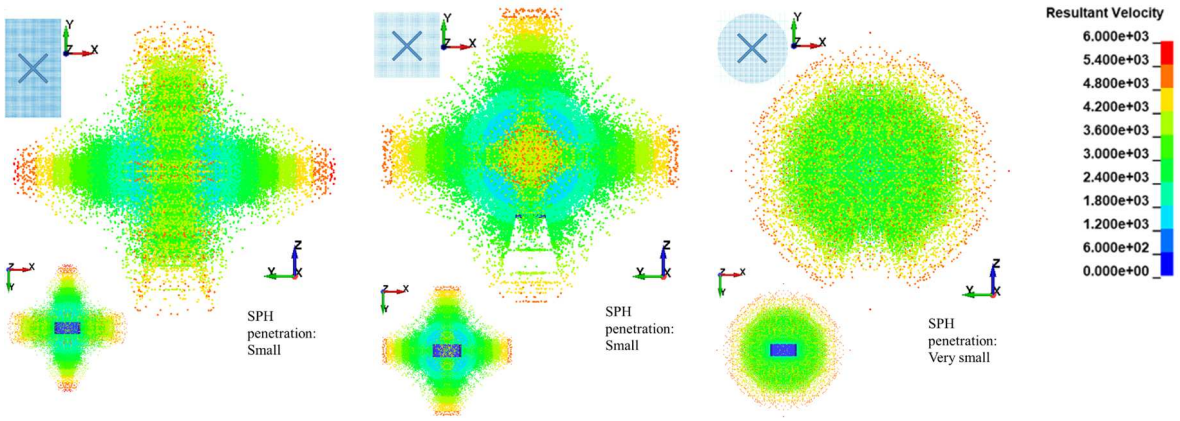

(a) Cyl. 100 #mid, αx0, αy90 (b) Cube #mid, αx0, αy0 (c) Sphere #mid, αx0, αy0 (d) Scale

Fig. 5 Resultant velocities of the SPH particles at time 500 μs after detonation, front and bottom views.

All the numerical analyses were calculated using Intel Xeon E5 1620 0 (Sandy Bridge-EP) 3.6 GHz, with a total number of 4 CPUs, using 4 SMP threads. The analysed cases are summarized in Tab. 1. The name of each case contains information about the TNT explosive shape (cylindrical, cubical, spherical), followed by the position of the initial detonation epicentre (#top or #mid), and the rotation of the explosive shape SPH grid, angles α_x, α_y as described in the previous chapter. The cases noted as "LBE" use the simplified blast method for the verification, and the 10 × 5 or 5 × 2.5 denotes the mesh density, as described in the previous chapter in detail.

The time step scale factor (tssfact) which decreases the default time step of the explicit analysis [2] was set as 0.2 for all the SPH analyses, and 0.9 for the LBE analyses. Hence, the time steps were $6.13 \cdot 10^{-8}$ s for the SPH analyses, and $2.76 \cdot 10^{-7}$ s, $2.3 \cdot 10^{-7}$ s for the LBE calculations (default time step is dependent on the mesh size, with finer step for the finer mesh). The second column of Tab. 1 informs about the actual physical calculation time, the mass of a single SPH node is denoted in the 3rd column, and the total SPH node number in the 4th. In some cases, e.g. if the time step is not fine enough with respect to the mesh density, penetration of SPH particles through the exposed slab might occur – as noted in the last column (see also Fig. 5 for insight, what is subjectively considered as "small penetration" by the authors of this study). If the time step is not sufficiently small, larger penetration might occur, as described in our previous, not yet published, research.

The results of all the analysed cases, mid-span displacement and reinforcement strain in time are depicted in Fig. 6 and Fig. 7 respectively, and provide insight into the sensitivity study of these variables on the explosive charge shape and orientation in the space.

DOI 10.13164/juniorstav.2024.24007

Tab. 1 Summary of analysed cases.

Case	Physical calculation time [h:m:s]	Mass of 1 SPH node [kg]	SPH number	SPH penetration
LBE 5 × 2.5	04:34:15	–	–	–
LBE 10 × 5	00:34:19	–	–	–
Cyl. 100 #mid, αx0, αy0	06:16:30	$1.6145 \cdot 10^{-6}$	247,753	small
Cyl. 100 #mid, αx0, αy90	05:12:36	$1.6145 \cdot 10^{-6}$	247,753	small
Cyl. 100 #top, αx0, αy90	05:38:36	$1.6145 \cdot 10^{-6}$	247,753	small
Cyl. 100 #mid, αx90, αy0	05:34:49	$1.6145 \cdot 10^{-6}$	247,753	small
Cyl. 100 #mid, αx45, αy45	05:08:43	$1.6145 \cdot 10^{-6}$	247,753	none
Cube #mid, αx0, αy0	05:32:22	$1.5259 \cdot 10^{-6}$	262,144	small
Cube #top, αx0, αy0	05:09:21	$1.5259 \cdot 10^{-6}$	262,144	small
Cube #mid, αx45, αy0	05:08:23	$1.5259 \cdot 10^{-6}$	262,144	very small
Cube #mid, αx0, αy45	05:19:48	$1.5259 \cdot 10^{-6}$	262,144	none
Sphere #mid, αx0, αy0	04:53:11	$1.6101 \cdot 10^{-6}$	248,439	very small
Sphere #top, αx0, αy0	05:02:40	$1.6101 \cdot 10^{-6}$	248,439	very small
Sphere #mid, αx45, αy0	04:58:16	$1.6101 \cdot 10^{-6}$	248,439	very small
Sphere #mid, αx0, αy45	05:17:03	$1.6101 \cdot 10^{-6}$	248,439	very small

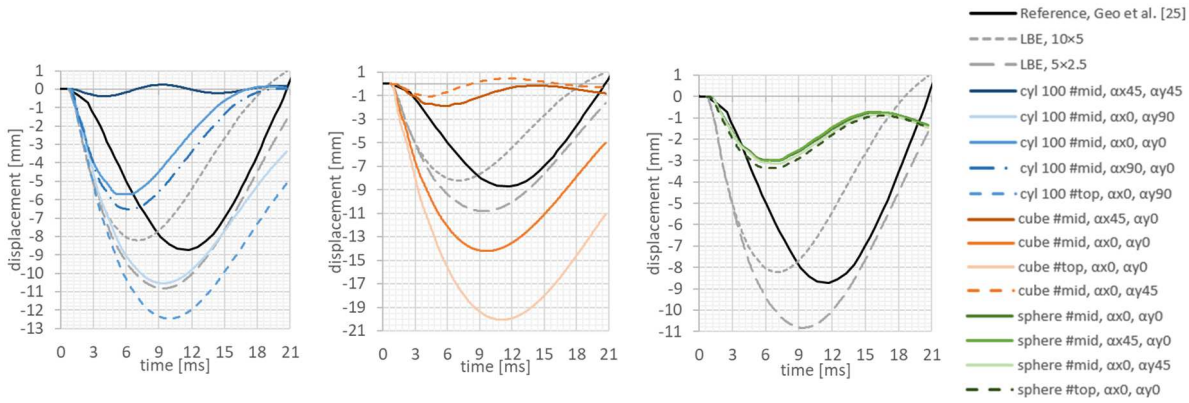

(a) Cylindrical TNT charges (b) Cubical TNT charges (c) Spherical TNT charges (d) Legend

Fig. 6 Sensitivity of the mid-span displacement in time on various charge shapes: reference data vs. analyses.

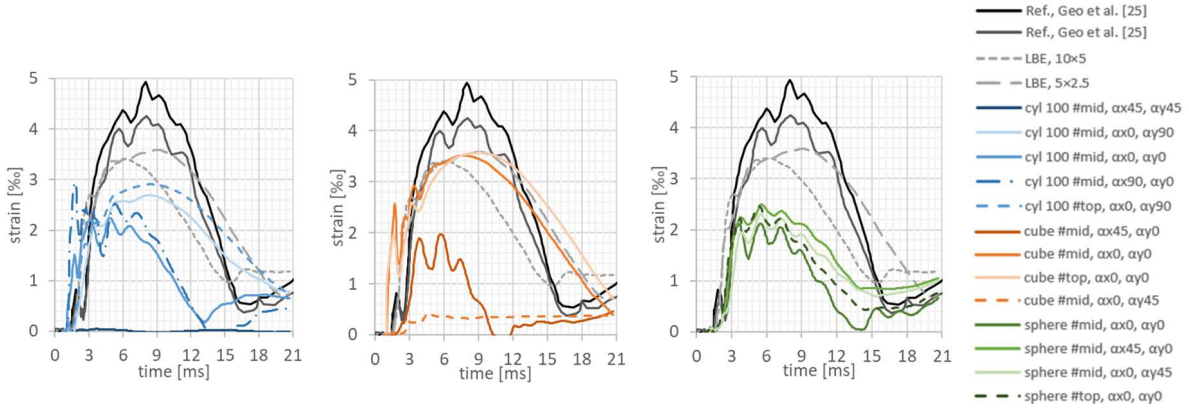

(a) Cylindrical TNT charges (b) Cubical TNT charges (c) Spherical TNT charges (d) Legend

Fig. 7 Sensitivity of the reinforcement strain in time on various charge shapes: reference data vs. analyses.

DOI 10.13164/juniorstav.2024.24007

4 DISCUSSION

With respect to the previous not yet published research study, a sufficiently small time step during the explicit analysis was selected, which was $6.13 \cdot 10^{-8}$ s for all the SPH analyses. This was achieved by setting the time step factor to 0.2 (for the considered geometry, material parameters and mesh density of the analysed structure). This time step resulted usually in very small penetration of the SPH particles through the exposed structure (Fig. 5, Tab. 1).

Significant dependence of the monitored variables on the shape and position of the explosive was observed: mid-span deflection in Fig. 6), and the axial reinforcement strain in the mid-span in Fig. 7. The smallest sensitivity of these variables was in the case of the various sphere rotations (Fig. 6 (c) and Fig. 7 (c)), which was expected, as the sphere explosive SPH grid was symmetric along the infinite axes in the macro-scale, but the discretization into regular cubical SPH grid (Fig. 4) introduced un-symmetry on the detailed scale.

Overall, considering the rather significant scatter of the monitored data, the results of the numerical analyses are in nice match with the experimental data, the initial slope of the strain, so-called strain rate, is approximately the same for all the analysed cases (Fig. 7). The best match in the maximal reinforcement strain between analysis and experiment is observed in case of the cubical SPH charge (Fig. 7 (b)), or cases of the simplified blast model LBE. Analogical conclusion might be done with the mid-span displacements (Fig. 6). Note: the case of a cylinder rotated $\alpha_x = \alpha_y = 45°$ (Cyl. 100 #mid, αx45, αy45) results in almost zero displacement and strain, as this rotation of the explosive volume directed almost all the SPH particles in trajectory to avoid contact with the exposed slab.

Basic sensitivity study is presented in this paper. More detailed study which considers various uncertainties of the model is presented by Hušek et al. [37] which considers different geometry and loading conditions of the exposed structure.

5 CONCLUSIONS

This paper presented the numerical finite element analyses of a simply supported concrete slab with basalt fibre-reinforced polymer (BFRP) exposed to high-velocity pressure from close-range TNT detonation. Two approaches to the blast load modelling were used, simplified LBE for the verification, and the smoothed particle hydrodynamics method SPH. The main objective of this study was to investigate the influence of the explosive shape and its rotation on the monitored results of the mid-span displacement and reinforcement strain of the exposed slab. A basic sensitivity study of these monitored outputs on the explosive charge's initial shape and rotation (defined by two angles in 3D) was conducted. Variously rotated cylinders, cubes and spheres were analysed.

The performances of all the model cases were graphically compared with each other and the experimental data was based on the research of fellow scientists (Gao et al. [25]). Overall good matches have been achieved.

As the input parameters of this sensitivity study are shapes and rotations of the explosive charge, the results might be applicable to the structure of any material (steel, wood, polymer). Significant dependency on these input parameters has been observed, with the best match for either cubical explosive, or certainly rotated cylinder. Further research into this topic will be conducted.

Acknowledgement

This paper has been created with the financial support of the Czech Science Foundation Project No.: 23-04712S and project FAST-J-23-8299 provided by the Brno University of Technology fund for specific university research.

References

[1] KRÁLIK, J. Safety of nuclear power plant against the aircraft attack. *Applied Mechanics and Materials*. 2014, vol. 617, pp. 76–80, DOI 10.4028/www.scientific.net/AMM.617.76

[2] LS-Dyna Theoretical manuals [product manual]. In: LS-Dyna Support [online]. ©2024 Dynamore GmbH [accessed: 1.11.2023]. Available at: https://www.dynasupport.com/manuals

[3] RANDERS-PEHRSON, G., K.A. BANISTER. Airblast loading model for DYNA2D and DYNA3D. Army Research Laboratory. 1997, Report. ARL-TR-1310, U.S. Available at: https://apps.dtic.mil/sti/tr/pdf/ADA322344.pdf

[4] FRIEDLANDER, F.G. The diffraction of sound pulses I. Diffraction by a semi-infinite plane. *Proceedings of the Royal Society A*. 1946, ISSN 0080-5630. DOI 10.1098/rspa.1946.0046

[5] KARLOS, V., G. SOLOMOS. Calculation of blast loads for application to structural components. *JRC*

Technical Reports. 2013, Report EUR 26456 EN, Luxembourg. ISSN 1831-9424. DOI 10.2788/61866

[6] LEE, E., J. HORNING, J. KURY. Adiabatic expansion of high explosives detonation products. *Lawrence Livermore National Laboratory*. 1968, University of California, Livermore, TID 4500-UCRL 50422.

[7] LEE, E., M. FINGER, W. COLLINS. JWL equation of state coefficients for high explosives. *Lawrence Livermore National Laboratory*. 1973, University of California, Livermore, Report UCID-16189.

[8] DOBRATZ, B.M. LLNL explosives handbook: properties of chemical explosives and explosives and explosive simulants. *Lawrence Livermore National Laboratory*. 1981, DOI10.2172/6530310

[9] KINNEY, G.F., K.J. GRAHAM. *Explosive shocks in Air*. Springer-Verlag Berlin Heidelberg, 1985. ISBN: 978-3-642-86682-1. DOI 10.1007/978-3-642-86682-1

[10] TABATABAEI, Z.S., J.S. VOLZ. A comparison between three different blast methods in LS-Dyna®: LBE, MM-ALE, Coupling of LBE and MM-ALE [online]. Presented at: *12th International LS-Dyna® Users Conference*. 2012, Detroit, US [accessed: 1.11.2023]. Available at: https://www.dynalook.com/conferences

[11] SLAVIK, T. A coupling of empirical explosive blast loads to ALE air domains in Ls-Dyna® [online]. Presented at: *7th European LS-Dyna® Conference*. 2009, Salzburg, Austria [accessed: 1.11.2023]. Available at: https://www.dynalook.com/conferences

[12] GINGOLD, R.A., J.J. MONAGHAN. Smoothed particle hydrodynamics: theory and application to non-spherical stars. *Monthly Notices of the Royal Astronomical Society.* 1977, vol. 181, is. 3, pp. 375–389 ISSN 1365-2966. DOI 10.1093/MNRAS/181.3.375

[13] LUCY, L.B. A numerical approach to the testing of the fission hypothesis. *The Astronomical Journal*. 1977, vol. 82, pp. 1013–24. ISSN: 0004-6256. DOI 10.1086/112164

[14] LIBERSKY, L.D., P.W. RANDLES, T.C. CARNEY, D.L. DICKINSON. Recent improvements in SPH modeling of hypervelocity impact. *International Journal of Impact Engineering*. 1997, vol. 20, is. 6–10, pp. 525–532. ISSN: 0734-743X. DOI 10.1016/S0734-743X(97)87441-6

[15] PRAMANIK, R., D. DEB. Implementation of smoothed particle hydrodynamics for detonation of explosive with application to rock fragmentation. *Rock Mechanics and Rock Engineering*. 2015, 48, pp. 1683–1698. DOI 10.1007/s00603-014-0657-y

[16] CHEN, J.Y., F.S. LIEN. Simulations for soil explosion and its effects on structures using SPH method. *International Journal of Impact Engineering*. 2018, vol. 112, pp. 41-51. ISSN: 0734-743X. DOI 10.1016/j.ijimpeng.2017.10.008.

[17] SCHWER, L., T. HAILONG, S. MHAMED. LS-Dyna Air Blast Techniques: Comparisons with Experiments for Close-in Charges [online]. Presented at: *10th European LS-Dyna® Conference*. 2015, Würzburg, Germany [accessed: 1.11.2023]. Available at: https://www.dynalook.com/conferences

[18] TRAJKOVSKI, J. Comparison of MM-ALE and SPH methods for modelling blast wave reflections of flat and shaped surfaces [oline]. Presented at: *11th European LS-Dyna® Conference*. 2017, Salzburg, Austria [accessed: 1.11.2023]. Available at: https://www.dynalook.com/conferences

[19] MALVAR, L.J., C.A. ROSS. Review of strain rate effects for concrete in tension. *American Concrete Institute Materials Journal.* 1998, 95(6), pp. 735–739. DOI 10.14359/418

[20] TAI, Y.S., T.L. CHU, H.T. HU, J.Y. WU. Dynamic response of a reinforced concrete slab subjected to air blast load. *Theoretical and Applied Fracture Mechanics.* 2011, vol. 56, issue. 3, pp. 140–147. ISSN 0167-8442. DOI 10.1016/j.tafmec.2011.11.002

[21] ZHAO, C.F., J.Y. CHEN. Damage mechanism and mode of square reinforced slab subjected to blast loading. *Theoretical and Applied Fracture Mechanics.* 2013, vol. 63-64, pp. 54-62. ISSN 0167-8442. DOI 10.1016/j.tafmec.2013.03.006

[22] ZHAO, C.F., J.Y. CHEN, Y. WANG, S.J. LU. Damage mechanism and response of reinforced concrete containment structure under internal blast loading. *Theoretical and Applied Fracture Mechanics*. 2012, vol. 61, pp. 12–20. ISSN 0167-8442. DOI 10.1016/j.tafmec.2012.08.002

[23] THIAGARAJAN, G., A.V. KADAMBI, S. ROBERT, C.F. JOHNSON. Experimental and finite element analysis of doubly reinforced concrete slabs subjected to blast loads. *International Journal of Impact Engineering*. 2015, vol. 75, pp. 162–173. ISSN 0734-743X. DOI 10.1016/j.ijimpeng.2014.07.018

[24] DUBEC B., P. MANAS, J. STOLLER, P. STONIS. Experimental and numerical assessment of fibre reinforced concrete slab under blast load. At*: ICMT 2019 – 7th International Conference on Military Technologies, Proceedings 2019*. ISBN: 978-172814593-8. DOI 10.1109/MILTECHS.2019.8870129

[25] GAO, Y., Y. ZHOU, J. ZHOU, X. KONG, B. ZHANG, S. LIU, J. FENG, N. ZHU, H. FAN and F. JIN. Blast responses of one-way sea-sand seawater concrete slabs reinforced with BFRP bars. *Construction and Building Materials*. 2020, vol. 232, 117254. DOI 10.1016/j.conbuildmat.2019.117254

[26] CRAWFORD, J.E., L.J. MALVAR. User's and Theoretical Manual for K&C Concrete Model. *Karagozian & Case Structural Engineers.* 1997, Glendale, CA. Report No. TR-97-53.1

[27] MALVAR, L.J., Review of Static and Dynamic Properties of Steel Reinforcing Bars. *American Concrete*

Institute Materials Journal. 1998, 95(5), pp. 609–616. DOI 10.14359/403

[28] FENG, J., Y. ZHOU, P. WANG, B. WANG, J. ZHOU, H. CHEN, H. FAN, F. JIN. Experimental research on blast-resistance of one-way concrete slabs reinforced by BFRP bars under close-in explosion. *Engineering Structures*. 2017, vol. 150, pp. 550–561. ISSN: 0141-0296. DOI 10.1016/j.engstruct.2017.07.074

[29] HOPKINSON, B. Rep. 13565. *British Ordnance board minutes*. 1915, British Ordnance Office, London.

[30] CRANZ, C. *Lehrbuch der Ballistik. Erster Band. Ausere Balistik*. Berlin: Springer Verlag, 1925. Available at: https://www.mori.bz.it/Balistica/Cranz%20%20-%20Aussere%20Ballistik%20I%20-1925.pdf

[31] MALVAR, L.J., J.E. CRAWFORD, J.W. WESEWICH, D. SIMONS. A New Concrete Material Model for DYNA3D. *Karagozian & Case Structural Engineers*. 1994, Glendale, CA. Report to the Defense Nuclear Agency No. TM-94-14.3

[32] MALVAR, L.J., J.E. CRAWFORD, J.W. WESEWICH, D. SIMONS. A New Concrete Material Model for DYNA3D – Release II: Shear Dilation and Directional Rate Enhancements. *Karagozian & Case Structural Engineers*. 1996, Glendale, CA. Report to the Defense Nuclear Agency No. TR-96-2.2

[33] MALVAR, L.J., J.E. CRAWFORD, K.B. MORRILL. K&C concrete material model release III – automated generation of material model input. *Karagozian & Case Structural Engineers*. 2000, Glendale, CA. Report to the Defense Nuclear Agency No. TR-99-24-B1

[34] MAGALLANES, J.M., Y. WU, L.J. MALVAR, J.E. CRAWFORD. Recent Improvements to Release III of the K&C Concrete Model [online]. At: *11th International LS-Dyna Users Conference*. 2010, Detroit, US [accessed: 1.11.2023]. Available at: https://www.dynalook.com/conferences

[35] CRAWFORD, J.E., Y. WU, H.J. CHOI, J.M. MAGALLANES, S. LAN. Use and Validation of the Release III K&C Concrete Material Model in LS-Dyna. *Karagozian & Case Structural Engineers*. 2012, Glendale, CA. Public report no. TR-11-36.6

[36] CHEN, W.F., D.J. HAN. *Plasticity for structural engineers*. New York: Springer Verlag 1988. ISBN 978-0387967110

[37] HUSEK, M., KALA, J. Uncertainties in blast simulations evaluated with Smoothed Particle Hydrodynamics method. *Structural Engineering and Mechanics*. 2020, vol. 74, pp. 771–787. DOI 10.12989/sem.2020.74.6.771